Thyroid hormones maintain parvalbumin neuron functions in mouse neocortex

Juan Ren[1, 2], Suzy Markossian[1], Romain Guyot[1], Denise Aubert[1], Dongdong Li[3], Bruno Cauli[3], Fabrice Riet[4], Jiemin Wong[5], Frédéric Flamant[1,*], Sabine Richard[1]

[1] Ecole Normale Supérieure de Lyon, INRAE, CNRS, Institut de Génomique Fonctionnelle de Lyon, 69364 Lyon, France

[2] East China Normal University, Shanghai, China

[3] Sorbonne Université, CNRS, INSERM, Neurosciences Paris Seine - Institut de Biologie Paris Seine (NPS-IBPS), 9 quai Saint Bernard, 75005 Paris, France.

[4] CNRS, INSERM, CELPHEDIA, PHENOMIN, Institut Clinique de la Souris (ICS), Université de Strasbourg, 1 rue Laurent Fries, 67404, Illkirch Graffenstaden, France

[5] Shanghai Key Laboratory of Regulatory Biology, Institute of Biomedical Sciences and School of Life Sciences, East China Normal University, Shanghai, China

[*] Corresponding author. Frederic.flamant@ens-lyon.fr Tel: 00 (33) 4 26 73 13 32

Summary

Parvalbumin-expressing (PV) GABAergic interneurons play a key role in maintaining the excitation-inhibition balance in the mammalian neocortex. Here we address the function of thyroid hormones in PV neurons in the mouse neocortex. To this end, Cre/loxP recombination system was used to express a dominant negative mutated receptor of thyroid hormones only in PV neurons. We analyzed the neocortical phenotype of these mice, in which thyroid hormone signaling is eliminated specifically in PV neurons, by combining genomics, histology, electrophysiology, and behavioral analysis. We found significantly altered gene expression, reduced expression of key perineuronal net components, reduced PV neuron excitability, behavioral hyperactivity and increased susceptibility to seizures. These results highlight that thyroid hormones are not only required for the differentiation of PV interneurons, but also for the maintenance of their inhibitory function after the onset of parvalbumin expression.

Keywords

Thyroid hormone/nuclear receptor/cortex/parvalbumin

Introduction

The dynamic balance between excitatory and inhibitory neurotransmissions plays a fundamental role in the function of neocortical neuronal circuits in mammals (Sohal and Rubenstein, 2019). The inhibitory GABAergic interneurons account for approximately 15% of the neuronal population of the neocortex (Rudy et al., 2011). They control the excitatory signaling of neighboring pyramidal neurons and prevent runaway feed-forward excitation. PV neurons are the most common subtype of neocortical GABAergic interneurons, with the proportion of approximately 40%. Neocortical PV neurons have a fast-spiking phenotype and are recognized by the expression of the parvalbumin protein(Hu et al., 2014).

The appearance of parvalbumin in the neocortex, which occurs during the first postnatal weeks in mice(del Rio et al., 1994), is a relatively late event of neocortical circuit maturation. It is highly dependent on the presence of thyroid hormones (TH) (Berbel et al., 1996). TH (thyroxine, or T4, and 3,3',5-triiodo-L-thyronine, or T3, its active metabolite) mainly act by binding to nuclear receptors called TRα1, TRβ1, and TRβ2, which are encoded by the *Thra* and *Thrb* genes in mice. These receptors, collectively called TRs, act as TH-dependent transcription factors, activating the expression of neighboring genes. *Thra* mutations are suggested to have dramatic consequences on development, notably neurodevelopment (Chatonnet et al., 2011). In the neocortex, the most visible consequence of *Thra* mutations is a dramatic impairment of PV neuron maturation (Richard et al., 2020; Wallis et al., 2008). When selectively expressed in GABAergic neurons from fetal stages, the TRα1^{L400R} mutated receptor causes epileptic seizures and mice die within three weeks after birth (Richard et al., 2020).

Currently, it is unclear whether the requirement for TH persists in PV neurons once their maturation is complete. The alternative would be that TH is necessary for PV neurons only during a short postnatal period, and that any alteration would have long lasting consequences. Here, we address this question by using the mouse model in which a mutated *Thra* allele, *Thra*^{AMI}, drives the expression of the TRα1^{L400R} dominant-negative receptor exclusively in PV neurons. This led to a specific blockade of TH signaling in PV neurons after the onset of PV expression. Unlike mice that express this mutation at an earlier stage in all GABAergic neurons (Richard et al., 2020) *Thra*$^{AMI/+}$ *Pvalb-Cre* mice were viable and did not display any major neurological defect. Multiscale phenotyping, which combined genomic, histological, electrophysiological, and behavioral observations, revealed alterations in the functions of neocortical PV neurons. These observations demonstrate that TH signaling in PV neurons is required

not only for proper differentiation of these neurons, but also for maintaining their functions in the adult neocortex.

Results

Genomic consequences of TRα1^{L400R} expression in PV neurons

Our first aim was to analyze the long term and cell autonomous consequences of the inhibition of T3 response in PV neurons, using gene expression analysis. Therefore, we combined the floxed *Thra^{AMI} and Pvalb-Cre* transgenes with the *ROSA-GSL10gfp^{lox}* reporter construct (Supplementary Fig. 1), which produces a green fluorescent protein in the nuclei of PV neurons after Cre/loxP recombination. Fluorescent cell nuclei were sorted from the neocortex of adult mice, differing by the expression of the dominant-negative TRα1^{L400R} in PV neurons (*Thra$^{AMI/+}$ ROSA-GSL10gfp$^{lox/+}$ Pvalb-Cre* mice vs *Thra$^{+/+}$ ROSA-GSL10gfp$^{lox/+}$ Pvalb-Cre* control littermates). RNA was extracted from the sorted nuclei and used for RNA-seq. Differential gene expression analysis identified 281 genes whose expression was either increased or decreased in PV neurons (Fig. 1a).

We then attempted to make a distinction among these 281 genes between the TR target genes, whose transcription is normally up-regulated by the liganded TRs, and the genes whose deregulation is only secondary to the long term expression of TRα1^{L400R}. To address this question, we searched for genes whose expression is rapidly modified in PV neurons when adult hypothyroid mice are treated with TH. Hypothyroidism was induced in a group of adult *ROSA-GSL10gfp$^{lox/+}$ Pvalb-Cre* mice by a prolonged pharmacological treatment. Some of these hypothyroid mice then received a single intraperitoneal injection of TH to restore the circulating level of TH, and gene expression was analyzed 24 hours later. In this setting, TH response takes place in all cell types and influences gene expression in PV neurons both directly and indirectly, as it modifies their microenvironment. In sorted nuclei of PV neurons, only a few genes behaved like *bona fide* TR target genes, being equally sensitive to hypothyroidism and TRα1^{L400R} expression, while sensitive to TH treatment (Fig. 1b, c and Supplementary data). Notably, the expression of the *Hr* gene, which is a well-known TR target gene, was not restored by TH treatment. This probably stems from the fact that TH do not efficiently cross the blood-brain barrier. Of note, the statistical filters that we have used to identify TR target genes are very stringent, so that the transcriptome analysis that we performed probably underestimates the number of TR target genes in PV neurons.

Another approach to pinpoint TR target genes would be to identify the TR binding sites (TRBS) in chromatin. As we could not directly address chromatin occupancy by TRs in PV neurons by ChIP-seq

analysis, because of the limited amount of chromatin extracted from sorted nuclei, we chose an indirect approach, relying on the fact that chromatin opening occurs in a ligand-dependent manner near the TRBS (Cho et al., 2023; Ng et al., 2023). We thus used Atac-seq to assess the influence of TH on chromatin accessibility in PV neurons (Fig. 1d). Differential data analysis (hypothyroid mice vs hypothyroid mice treated with TH) identified 11 207 differentially accessible sites (DAS), representing ∼25% of all the detected accessible sites. However, the set of genes located near the DAS (< 30 kb), was not enriched in TH-responsive genes, as defined above. This suggests that only a fraction of DAS is associated to TRBS, and that Atac-seq alone is not sufficient to identify TR target genes.

In order to predict the position of at least some of the TRBS in PV neurons, we assumed that a fraction of these would be shared across cell types, as indicated by a recent atlas of Chip-seq datasets (Zekri et al., 2022). We thus extracted from the 18 064 TRBS present in striatum GABAergic neurons, 4181 sites that are shared by these GABAergic neurons and at least one another unrelated cell type (cardiomyocyte, hepatocyte, or adipocyte). We then focused on 1013 of these 4181 TRBSs that overlap with the previously defined DAS in PV neurons (called TRBS/DAS). This allowed to pinpoint 12 genes (*Galnt14, Rhobtb2, Kmt5c, Rgcc, Nudt7, Ece1, Ampd2, Gpr83, Sema7a*, *Arl4d, Bhlhe40, Zfp691*) that fulfill two criteria indicating that they are TR target genes: they are downregulated in *Thra*$^{AMI/+}$ *ROSA-GSL10gfp*$^{lox/+}$ *Pvalb-Cre* mice according to RNA-seq, and their transcription start site is located within 30 kb of a TRBS/DAS. Importantly, none of the TRBS/DAS was located near a gene up-regulated in TRα1^{L400R} expressing PV neurons or down-regulated by TH, which is consistent with the fact that liganded TRs activate transcription.

The 281 genes whose expression is deregulated in TRα1^{L400R} expressing PV neurons have various known functions in signal transduction, ion exchanges and enzymatic activities. Thirty one of them (11%) encode proteins that are found in the extracellular domain, mainly extracellular matrix components, among which several are likely TR target genes (*Acan, Npnt, Sema7a, Vash2, Tesc*). This suggests a possible defect of the perineuronal net (PNNs), a specialized and highly glycosylated extracellular matrix that surrounds many cortical PV neurons. PNNs provide PV neurons with a mesh-like structure accommodating numerous synaptic terminals, a physical barrier between the neuronal surface and the extracellular space, and its diverse interacting molecules. These functions allow PNNs to regulate the plasticity of PV neurons (Sorg et al., 2016).

Histological consequences of TRα1^{L400R} expression in PV neurons

PV neurons display a marked sensitivity to alterations in TH signaling during brain development (Richard et al., 2020). We thus set out to study if the density of PV neurons in the adult mouse

neocortex differed between *Thra*$^{AMI/+}$ *ROSA-tdTomato*$^{lox/+}$ *Pvalb-Cre* mice (n = 9) and *Thra*$^{+/+}$ *ROSA-tdTomato*$^{lox/+}$ *Pvalb-Cre* control littermates (n = 7), which produce a red fluorescent protein in the cytoplasm of PV neurons after Cre/loxP recombination. Immunohistochemistry was performed to label parvalbumin and Wisteria floribunda Agglutinin (WFA) was used to label N-acetyl-galactosamine-β1 residues of PNN glycoproteins in the somatosensory cortex.

We found no difference between the two groups of mice in the density of Tomato-expressing cells (Fig. 2a, b), which indicates that the expression of TRα1^{L400R} did not compromise the viability of the targeted cells, namely PV neurons. Compared to controls, mutant mice exhibited a slightly, but significantly, higher density of parvalbumin-expressing cells (Fig. 2a, c), accompanied by a slightly, but significantly lower ratio of parvalbumin-expressing cells that were surrounded by PNNs (Fig. 2a, e). Thus, unlike what we have previously observed with a Cre driver expressed from a prenatal stage in all GABAergic neurons (Richard et al., 2020), the differentiation of PV neurons is not drastically altered in *Thra*$^{AMI/+}$ *ROSA-tdTomato*$^{lox/+}$ *Pvalb-Cre* mice. Since PNNs surrounding PV neurons allow them to regulate plasticity, the above results suggest that TH signaling might be of physiological importance in PV neurons.

Electrophysiological consequences of TRα1^{L400R} expression in PV neurons

The fact that TRα1^{L400R} expression in PV neurons deregulated genes encoding PNN components and ions channels, and reduced the density of PV neurons surrounded by PNNs, prompted us to evaluate the electrophysiological properties of PV neurons expressing TRα1^{L400R}. Whole-cell current-clamp recording was performed on acute slices of the somatosensory cortex, which were prepared from 16-to-24-day-old *Thra*$^{AMI/+}$ *ROSA-tdTomato*$^{lox/+}$ *Pvalb-Cre* mice (n = 10) and *Thra*$^{+/+}$ *ROSA-tdTomato*$^{lox/+}$ *Pvalb-Cre* control littermates (n = 8). Current steps were injected to fluorescent cells, and voltage responses were recorded (Fig. 3a, b). In the end, 35 mutant FS-PV neurons and 19 control cells were recorded, and 37 parameters were measured for each cell (Karagiannis et al., 2009) in accordance with Petilla terminology (Ascoli et al., 2008). This allowed for a comprehensive analysis of the electrophysiological behavior of each recorded PV neuron (Supplementary Table 1).

Recorded neurons displayed the archetypal properties of fast-spiking PV neurons, with a relatively low membrane resistance, short spikes with sharp after-hyperpolarizations (AHPs), and an ability to fire

action potentials (APs) at a high firing rate with little or no frequency adaptation (Fig. 3a, b and supplementary table 1). Three parameters differed significantly in the PV neurons of *Thra*$^{AMI/+}$ *ROSA-tdTomato*$^{lox/+}$ *Pvalb-Cre* mice, compared to controls. The first one was the rheobase (Fig. 3c), which is the minimal depolarizing current pulse intensity generating at least one action potential. The rheobase was significantly higher in mutant PV neurons. The two other parameters that were also higher in mutants were the thresholds of the first and second APs generated by a rheobasic current injection (Fig. 3d). Collectively, these alterations indicate that PV neurons expressing TRα1^{L400R} exhibit a lower excitability.

Behavioral consequences of TRα1^{L400R} expression in PV neurons

The results reported above show that gene expression, extracellular matrix glycosylation and electrophysiological properties are significantly altered in the neocortical PV neurons of *Thra*$^{AMI/+}$ *Pvalb-Cre* mice, which might result in an alteration of the excitation-inhibition balance in the neocortex. We thus explored the possible behavioral consequences of *TRα1*^{L400R} expression in PV neurons. Two groups of adult females, *Thra*$^{AMI/+}$ *Pvalb-Cre* mice and *Thra*$^{+/+}$ *Pvalb-Cre* control littermates, underwent a series of behavioral tests (Supplementary Table 2).

The most salient observation was that *Thra*$^{AMI/+}$ *Pvalb-Cre* mice exhibited a higher level of general activity. They traveled significantly higher distances than control mice in the open-field, novel object recognition as well as social interaction tests (Fig. 4a, Supplementary Table 2). Moreover, in the acquisition phase of the test for novel object recognition, they spent significantly more time exploring objects (Fig. 4d). Finally, in the marble burying test, they buried significantly more marbles than controls (Fig. 4e). This reflects a higher level of digging behavior, which is a typical behavior that mice display when they are provided with sufficient substrate to displace (Deacon, 2006).

We next addressed the susceptibility of *Thra*$^{AMI/+}$ *Pvalb-Cre* mice to an epileptogenic drug, the GABA receptor antagonist pentylenetetrazole. In this test, they displayed more frequent and more severe seizures than controls (Fig. 4g).

Assessment of cognitive abilities revealed that, in spite of good learning abilities, *Thra*$^{AMI/+}$ *Pvalb-Cre* mice exhibited less behavioral flexibility than controls. In the test for novel object recognition, control and mutant mice demonstrated a similar ability to discriminate a novel object from a known object (Fig. 4d). In a touch screen test, there was no difference between genotypes in visual discrimination learning (Fig. 4c). However, adapting to a change in the rule proved to be more difficult for mutant mice. In the reversal learning phase, mutant mice reached the learning criterion (% of correct

responses higher than chance) during the 10th session, whereas control mice reached the criterion during the 9th session (Fig. 4c).

In a social interaction test, *Thra*$^{AMI/+}$ *Pvalb-Cre* mice initiated significantly more social approaches and contacts (Fig. 4f, Supplementary Table 2). However, the mean duration of social contacts initiated by mutant mice was shorter, so that the total contact duration did not differ between genotypes. Thus, the higher numbers of social approaches and contacts in mutant mice appear to reflect their higher level of general activity rather than a higher degree of social motivation.

Thra$^{AMI/+}$ *Pvalb-Cre* mice did not show any overt sign of increased anxiety. They spent the same amounts of time as controls in anxiogenic parts of test devices: open arms in the elevated-plus maze test (Fig. 4b), center of the arena in the open-field and social interaction tests (Supplementary Table 2).

Discussion

We present here experiments which demonstrate that in the mouse brain, TH signaling is required in PV neurons after they express the *Pvalb* gene. This expression starts in a protracted manner, at different time points in different neocortical areas, after the first postnatal week (de Lecea et al., 1995). Blocking TH signaling in PV neurons alters the expression of a small set of genes. Changes in gene expression do not compromise the survival of PV neurons but have adverse consequences on the elaboration of PNNs, PV neuron excitability and mouse behavior.

The mild consequences of expressing TRα1^{L400R} in PV neurons in *Thra*$^{AMI/+}$ *Pvalb-Cre* mice contrast with the postnatal lethality caused by epileptic seizures observed in mice with the *Gad2-Cre* transgene driving the same mutation in all GABAergic neurons from embryonic day 12.5 (Richard et al., 2020). This previous study indicates that, compared to other cortical GABAergic neuron subtypes, PV neurons are, by far, the most sensitive to this early TRα1^{L400R} expression. Therefore, the decreased severity of the phenotype observed in *Thra*$^{AMI/+}$ *Pvalb-Cre* mice, compared to *Thra*$^{AMI/+}$ *Gad2-Cre* mice, is likely to result from the later inhibition of TH signaling in PV neurons, rather than from its restriction to a fraction of the GABAergic neuronal population. Indeed, to our knowledge there is no evidence to support the possibility that TH signaling indirectly impacts PV neuron development, through the regulation of target genes in neighboring GABAergic neurons. Thus, the most likely interpretation of the difference observed between *Thra*$^{AMI/+}$ *Pvalb-Cre* mice and *Thra*$^{AMI/+}$ *Gad2-Cre* mice is that TH signaling plays a major role for PV neuron differentiation before the onset of *Pvalb* expression, but is also required for the lifelong maintenance of specific characteristics of PV neurons.

The behavioral phenotype of mice expressing TRα1^{L400R} only in PV neurons was mainly characterized by a general increase in general activity, reduced behavioral flexibility and an increased susceptibility to pentylenetetrazole-induced seizures. The susceptibility to epilepsy is an indication of an increase in the excitation-inhibition balance in neocortical circuits, a feature observed in many neuropsychiatric disorders (Rubenstein and Merzenich, 2003; Sohal and Rubenstein, 2019). These behavioral defects differ notably from those reported for mice expressing TRα1^{R384C} in the whole body. These have been reported to display high anxiety, memory defects (Venero et al., 2005; Wallis et al., 2010) and reduced seizure susceptibility (Hadjab-Lallemend et al.). TRα1^{R384C} possesses a residual sensitivity to T3, and its expression only delays PV neuron differentiation. Treating adult mice with high doses of TH only partially normalizes their behavior, suggesting that part of the observed alterations are irreversible consequences of neurodevelopmental defects. TH also exert a cell-autonomous influence on adult excitatory cortical neurons, and the selective inhibition of TH signaling in these neurons also has visible consequences on behavior (Hochbaum et al., 2023). Finally, TRα1 mutations are also known to alter gene expression in glial cells (Picou et al., 2014). Therefore, the behavior traits observed in mice expressing TRα1^{R384C} reflect a combination of direct and indirect effects of the mutation, starting from developmental stage, in which the deregulation of gene expression in adult PV neurons is unlikely to play a major part.

The strength of the mouse model that we have used here is that it ascertains that the observed phenotype originates from a blockade of TH signaling in PV neurons and not from their microenvironment, which also has a major influence on their physiology. Therefore, the alteration of the PNN and the reduced excitability of PV neurons, are consequences of the gene deregulation caused by the prolonged expression of the TRα1^{L400R} receptor in these cells and are also most likely at the origin of the behavioral phenotype. Among many deregulated genes, we have identified a small subset, which are likely TR target genes and at the origin of the PV neurons phenotype. Among these are the *Acan, Sema7a* and *Nptn* genes that encode extra-cellular matrix proteins: aggrecan, a major component of the PNN, semaphorin 7a, which is anchored to the cell membrane, and nephronectin, an integrin-interacting glycoprotein. The deregulation of the *Galnt14* and *Has3* genes, encoding N-acetylgalactosaminyltransferase and hyaluronan synthase, respectively, might account for alterations of the carbohydrate portion of PNNs. However, more indirect mechanisms can also be at work. For example, down-regulation of *Me1, Ampd2* and *Nudt7* suggests alteration of the energy metabolism in PV neurons, which might translate into PNN defects. This hypothesis was put forward to explain the PNN phenotype of mice lacking the PGC1α TR coactivator in cortical GABAergic neurons (Zhang et al., 2023).

The electrophysiological phenotype of PV neurons expressing TRα1^{L400R}, mainly characterized by a reduced sensitivity to stimulation, is also the likely consequence of a combination of changes in the expression of several TR target genes. Although these electrophysiological properties might be related to PNN defects, additional molecular mechanisms might be involved. Among the identified TR target genes in PV neurons are *Tesc,* which encodes tescalcin, a calcium binding protein, and *Cacnb3* encoding a voltage-dependent calcium channel, which are likely to influence PV neuron electrophysiological properties.

In humans, adult onset of hypothyroidism may cause memory impairment, depression (Bode et al., 2021), forgetfulness, difficulty focusing and "brain fog" (Ettleson et al., 2022). However, concomitant fatigue, muscle weakness, bradycardia, and decrease in resting energy expenditure, which are of peripheral origin, can indirectly cause mood disorders. The current study highlights that the decrease in TH signaling in PV neurons account for at least some of the neurological symptoms caused by hypothyroidism.

Study limitations

The identification of TR target genes in PV neurons is incomplete, because we were not able to perform a Chip-Seq analysis to firmly establish the positions of TR binding sites in the genome, due to an insufficient amount of chromatin extracted from sorted PV neuron nuclei. Besides, we used the juvenile but not adult mice to do the electrophysiological experiments. In the end, more work is also needed to establish the link between the observed changes in gene expression and PV neuron defects.

Methods

Mouse models and treatments

Experiments involving the use of live animals for the current project were approved by local ethics committees (C2EA015 and C2EA017) and subsequently authorized by the French Ministry of Research (Projects #33279-2021082516194165 and #38581). Mice were bred and maintained at Plateau de Biologie Expérimentale de la Souris (SFR BioSciences Gerland - Lyon Sud, France).

The *Thra^{AMI}* allele allows the expression of the dominant-negative TRα1^{L400R} after the Cre/loxP-mediated deletion of a cassette with polyadenylation signals (Quignodon et al., 2007). The *ROSA-tdTomato^{lox}* reporter transgene (also known as Ai9, MGI Cat# 4436851, RRID: MGI: 4436851) drives the Cre-dependent expression of a red fluorescent protein (Madisen et al., 2010). The *ROSA-L10GSGfp^{lox}* transgene encodes the GS-EGFP-L10a protein, which is a green fluorescent protein fused to the N-

terminus part of the large subunit ribosomal protein L10a, mainly localized in cell nuclei. This transgene allows for a strong and specific staining of the nuclei (Heiman et al., 2008). The additional N-terminal GS tag, combines a fragment of protein G and a fragment of streptavidin suitable for protein purification (Burckstummer et al., 2006) . The entire reading frame and a drug-selection gene (NeoR) were inserted in the pHL-HH vector construct (Fehling et al., 2003) which contains 2 loxP sequences and 2 loxP^{2272} sequences (Heiman et al., 2008). The resulting vector was inserted into the ROSA26 locus of mouse embryonic stem cells by homologous recombination (Supplementary Fig. 1a). The combination of loxP and loxP^{2272} sites is organized so that Cre/LoxP recombination, taking place only between identical sequences, results in a two-step inversion/deletion (Supplementary Fig. 1b). This design allows the expression of GS-EGFP-L10a to be strictly dependent on Cre recombination (Fehling et al., 2003). All transgenes were in C57Bl6/J genetic background. *Pvalb-Cre* is a knock-in allele in which the Cre recombinase reading frame is inserted into the *Pvalb* gene in order to restrict the expression of the recombinase to PV neurons (Hippenmeyer et al., 2005). The *ROSA-tdTomato^{lox}* reporter system has allowed us to assess the specificity of PV neuron targeting. Of note, we have observed that in *ROSA-tdTomato$^{lox/+}$ Pvalb-Cre* mice, Cre-mediated recombination occurred not only in PV neurons throughout the brain, but also in cerebellar granule cells.

Mice were fed for 2 weeks with iodine deficient food supplemented with 0.15% of propyl-thio uracyl (Envigo ref TD.95125) to cause deep hypothyroidism. TH levels were restored by a single intraperitoneal injection in half of the animals (40 μg T4 + 4 μg T3 dissolved in 200 μL of phosphate buffer saline, all chemicals from Sigma Aldrich France). The other PTU treated animals were injected with 200 uL of phosphate buffer saline.

Nuclei sorting

Individual cortex were frozen in liquid nitrogen immediately after dissection. Samples were thawed and resuspended in 1.5 mL of lysis buffer (Nuclei EZ Lysis Buffer, Sigma, ref N 3408) and transferred in a 2 mL Dounce tissue grinder (Sigma ref D8938) for cell lysis (25 strokes with A pestle and 25 strokes with B pestle, on ice). Suspensions were transferred in tubes containing 2.5 mL of cold lysis buffer and centrifuged (5 min 500 g 4°C, swinging rotor). Supernatants were discarded and nuclei pellets were washed once with 4 mL Nuclei EZ Lysis Buffer and once with 4 mL of Nuclei Suspension Buffer (NSB) (PBS w/o Mg and Ca; 0.01% BSA; Biolabs ref B9000S; 40 U/mL RNAsin; Promega ref N251B). Final pellets were resuspended in 0.5 mL NSB containing DAPI (1 µL at 1 mg/mL) and were filtrated in tubes with 35 μm cell strainer (Corning, ref 352235). All pellets were resuspended by pipetting 10 times with 1 mL of buffer. For each condition, Fluorescence-Activated Cell Sorting (FACS Aria IIμ cytometer (BD))

was used to isolate all GFP positive nuclei. These were sorted in low binding Eppendorf tubes containing 0.5 mL NSB and centrifuged (5 min 20 000 g). Supernatants were discarded and nuclei pellet was resuspended in 350 µL RNA lysis buffer containing β-mercaptoethanol for RNA extraction (Qiagen RNeasy Microkit ref 74004).

RNA-seq analysis

Nuclear RNA was extracted from sorted nuclei (RNeasy Micro Kit, Qiagen ref 74004) and quantified using Tapestation 4150 (Agilent). 1 ng of RNA was reverse-transcribed using the SMART-Seq v4 Low Input RNA kit (Takara). cDNA were quantified and qualified using Qubit (Invitrogen) and Tapestation 4150 (Agilent). Libraries were then prepared from 1ng of cDNA using the Nextera XT DNA Library Kit (Illumina). Libraries were sequenced (> 2.10^7 reads/library) on a Nextseq500 DNA sequencer (Illumina). Reads were aligned on the mouse genome (mm10 GRCm38 release) with Bowtie2 (Galaxy Version 2.4.2 + galaxy 0) (Langmead et al., 2009). Count table was prepared using htseq-count (Galaxy Version 0.9.1 + galaxy 1, mode union, feature type: gene) (Anders et al., 2015). Differential gene expression analysis was performed with DEseq2 (Galaxy Version 2.1.8.3) (Love et al., 2014) using the following thresholds: False Discovery Rate < 0.05; p-adjusted value < 0.05; expression > 10 reads per million; fold-change > 1.5) . Hierarchical clustering was performed using Euclidian distance and Ward's distance with Clustvis (Metsalu and Vilo, 2015).

Atac-seq analysis

Cortex nuclei were purified as above and collected by centrifugation (500 g; 5 min) for immediate use in ATAC Library preparation (Tagmentase–loaded; Diagenode). The nuclei pellets were suspended in 25 µL 2xTagmentation Buffer (Diagenode) before addition of 22.5 µL of H_20 and 2.5 µL of Tn5 transposase. This mix was incubated under agitation (1400 rpm) for 30 min at 37°C. DNA fragments were purified using the MinElute PCR Purification Kit (Qiagen). The eluate (10 µL) was amplified by PCR after the addition of 12.5 µL H_20, 25 µL NEBNext® High-Fidelity 2xPCR Master Mix (New England Biolabs) and 2.5 µL of index primers (Nextera® XT Index kit v2; Illumina) as follows: 72°C for 5 min, 98°C for 30 s, followed by 5 cycles (98°C 10 s, 63°C 30 s, 72°C for 60 s). A preliminary qPCR was then performed with a fraction of the reaction product to determine the optimal number of amplification cycles needed for a second round of amplification without saturation: to this end 5 µL of iQ SYBR Green Supermix (Biorad) were added to 5 µL preamplified DNA and used for qPCR (98°C 30 s denaturation), followed by 20 cycles of amplification: (98°C 10 s, 63°C 30 s, and 72°C 60 s). The entire preamplified DNA was then amplified (usually 9–11 cycles). DNA from the final reaction was purified using 1.8x SPRI magnetic beads (Beckman Coulter) quantified with Qubit 4 fluorometer (Invitrogen) and qualified

using Tapestation 4150 (Agilent). Libraries were mixed in equimolar amounts and sequenced (> 2.10^8 reads/library; Nextseq500 DNA sequencer Illumina). Reads were aligned on the mouse genome (mm10 GRCm38 release) with Bowtie2 (Galaxy Version 2.4.2 + galaxy 0) (Langmead et al., 2009). Peaks were identified using MACS2 Galaxy Version 2.2.9.1 + galaxy 0). MACS2 was also used for differential occupancy analysis using a set of reference library to define background.

Brain slice collection

Each mouse was given a lethal intraperitoneal injection (6 mL/kg) of a mixture of ketamine (33 mg/mL) and xylazine (6.7 mg/mL). The thorax was opened and each mouse was perfused with 3.7% paraformaldehyde in 0.1 M phosphate buffer at room temperature. Each brain was dissected out, immersed in fixative at 4°C for 3 h and then in phosphate buffered saline (PBS) at 4°C until sectioning. Coronal sections (50 µm) were cut with the aid of a vibrating microtome (Integraslice 7550 SPDS, Campden Instruments, Loughborough, UK), in PBS at room temperature. Brain sections were stored at -20°C in cryoprotectant (30% ethylene glycol and 20% glycerol in 10 mM low-salt PBS).

Brain slice histology

Immunohistochemistry was performed on free-floating brain sections. For PV labeling, a mouse anti-PV primary antibody (PARV19, Sigma P3088, 1:2000), and a secondary antibody made in donkey (anti-mouse DyLight 633, ThermoFisher Scientific, 1:1000) were used. For the concurrent PNN labeling, a biotinylated Wisteria floribunda lectin (WFL/WFA, Vector Laboratories B-1355, 20 µg/mL), and Streptavidin coupled to DyLight 488 (Vector Laboratories, SA-5488, 1:1000) were used. Non-specific binding sites were blocked by incubating sections for 1 h in PBS with 1% BSA and 0.2% Triton X100. Brain sections were incubated overnight at 4°C with PV antibody and biotinylated WFA, which were diluted in PBS with 1% BSA, 0.2% Triton X-100 and 1% dimethyl sulfoxide. Sections were washed in PBS and further incubated for 15 min at room temperature with DAPI (4', 6-diamidino-2-phenylindole, 1:5000, Sigma). Incubation with the secondary antibody lasted for 3 h at room temperature. Sections were mounted in Fluoroshield™ (Sigma), coverslipped and imaged using an inverted confocal microscope (Zeiss LSM 780).

Image analysis

Image analysis was performed using ImageJ. Final images resulted from the z projection of 3 optical sections (Maximum intensity tool) that were 2 µm apart (the resulting images thus reflected the

fluorescence collected over a thickness of 4 µm). Tomato+, parvalbumin+ and PNN+ cells were counted with the Cell Counter in ImageJ plugin.

Slice preparation for electrophysiological recording

Juvenile mice (P16-P24) were deeply anesthetized with isoflurane and decapitated. The brains were quickly removed and placed into cold oxygenated artificial CSF (aCSF): 126 mM NaCl, 2.5 mM KCl, 1.25 mM NaH_2PO_4, 2 mM $CaCl_2$, 1 mM $MgCl_2$, 26 mM $NaHCO_3$, 10 mM glucose, 15 mM sucrose, and 1 mM kynurenic acid (nonspecific glutamate receptor antagonist; Sigma). Coronal slices (300 µm thick) from mouse somatosensory cortex were prepared as described previously (Karagiannis et al., 2009). Slices were cut with a vibratome (VT1000S; Leica), transferred to a holding chamber containing aCSF saturated with O_2/CO_2 (95%/5%), and held at room temperature.

Whole-cell electrophysiological recording. Individual slices were transferred to a submerged recording chamber and perfused (1–2 ml/min) with oxygenated aCSF. Patch pipettes (~10 MΩ) pulled from borosilicate glass were filled with 12 µl of internal solution: 144 mM K-gluconate, 3 mM $MgCl_2$, 0.5 mM EGTA, 10 mM HEPES, pH 7.2 (285/295 mOsm). Neurons were first identified in the slice by their tdTomato fluorescence and then patch under infrared differential interference contrast illumination (SliceScope Pro, Scientifica). Whole-cell recordings in current-clamp mode were performed at room temperature (24.5 ± 1.5°C) using a patch-clamp amplifier (MultiClamp 700B; Molecular Devices). Data were filtered at 10 kHz and digitized at 100 kHz using an acquisition board (Digidata 1440A; Molecular Devices) attached to a personal computer running pClamp 10.7 software package (Molecular Devices). All membrane potentials were corrected for theoretical liquid junction potential (-15.6 mV).

Behavior tests

Adult female *Thra*$^{AMI/+}$ *Pvalb-Cre* mice and *Thra*$^{+/+}$ *Pvalb-Cre* control littermates were transferred to PHENOMIN-ICS platform (Illkirch, France), where they underwent the following series of behavioral tests (Supplementary Table 2). 1.Open field: Each mouse was placed in the periphery of a 44*44 cm arena (Panlab, Barcelona, Spain), under 150 Lux illumination, and allowed to explore freely the apparatus for 30 min. The distance traveled, the number of rearings as well as the time spent in the central and peripheral regions were recorded (periphery width = 8 cm). 2. Elevated-plus maze: The apparatus comprised two open arms (30 X 5 cm) opposite one to the other and crossed by two closed arms (30 x 5 x 15 cm), all arms being equipped with infrared captors allowing automatic detection of the position of the mouse (Imetronic, Pessac, France). Mice were individually tested for 5 min. The following parameters were recorded: number of entries into and time spent in each arm, head dips,

rearings, stretched-attend posture. 3.Visual discrimination and reversal task: Mice were tested in Mouse Touch Screen Systems (Campden Instruments). In order to increase the motivation of the animals, the drinking water in the housing cages was acidified during test days. After pre-training to learn to touch an image that appeared on the screen in order to obtain a reward, mice were tested in a visual discrimination task. Touching the correct image was rewarded with strawberry milk (12% sucrose). Touching the incorrect image was punished with a timeout. Once the task was learnt, the correct image became incorrect and vice versa. Each animal performed a session of 1 hour maximum per day, involving up to 60 trials per session, during which the percentage of correct responses was recorded. 4. Novel object recognition: Mice were first habituated for 10 min in a closed circular arena (30 cm diameter and 50 cm height, homogeneously illuminated at 20 Lux). The next day, mice were submitted to a 10-min acquisition trial, during which they were placed in same the arena in presence of two identical objects (A). The time spent exploring the objects (sniffing) was manually recorded. Two hours later, mice were placed again in the same arena, where one of the objects had been replaced by a novel object (B). During this 10-min retention trial, the times spent exploring the objects (tA and tB) were recorded. A recognition index (RI) was defined as (tB / (tA + tB)) x100. Locomotor activity was recorded with EthoVision XT video tracking system (Noldus, Wageningen, Netherlands).5. Marble burying: Mice were tested individually for 15 minutes in a cage (Tecniplast GM500, illuminated at 25 lux) containing 3 cm high clean bedding and 20 black glass marbles (10 mm diameter) arranged in 5 lines of 4 marbles. EthoVision XT video tracking system (Noldus, Wageningen, Netherlands) was used for video recording. The number of marbles fully covered by bedding was measured every minute, between the 5th and 15th minutes of the test. 6. Social interaction with a Newcomer: Mice were tested in an open arena of 50*50 cm with sawdust. The animals were previously equipped with an RFID chip so that each animal could be tracked independently and its social behaviors recorded by the Live Mouse Tracker system (de Chaumont et al., 2019) . For the habituation session, the mouse under test was allowed to freely explore the arena for 20 minutes. An unknown female adult C57Bl/6 mouse (“newcomer”) was then placed in the arena for 30 min. The social behaviors, including social approaches, contacts, following the other mouse, were recorded as well as the distance traveled by each mouse. 7. Pentylenetetrazole-induced seizure: Each mouse received an intraperitoneal injection of pentylenetetrazole (with 40 mg/kg) and was placed in a translucent cage. Different types of seizures were manually recorded for 20 minutes following the injection: myoclonic (short jerking in parts of the body), clonic (periods of shaking or jerking parts on the body), tonic (muscles in the body become stiff).

Statistical analyses

Data are expressed as mean ± SEM. Data analyses were performed with Excel 2016 and GraphPad Prism software (v.8.). The level of significance was set at $p < 0.05$. For histological analysis, the densities of Tomato+, parvalbumin+, PNN+ cells, and their co-localizations were manually counted in the whole area of one image taken in the somatosensory cortex area. 3-4 images in each hemisphere were analyzed for each mouse. Quantitative data were analyzed using two-tailed unpaired T-test. In electrophysiological analysis, 37 parameters were manually defined as described (Karagiannis et al., 2009), adopting Petilla terminology (Ascoli et al., 2008). The normality was analyzed using Shapiro-Wilk test. Quantitative data were analyzed using Mann-Whitney test or unpaired T-test. For mouse behavior analysis, the normality was analyzed using Shapiro-Wilk test. Quantitative data were analyzed using two-tailed unpaired T-test or Mann-Whitney test and two-way ANOVA followed by Sidak's multiple comparisons test. For the comparison with chance, one group T-test was used. Outliers were identified with the ROUT method (Q = 1%). A Chi-square test was used to analyze the susceptibility to pentylenetetrazole-induced seizure.

Figure legends:

Fig. 1 | Changes in gene expression and chromatin condensation caused by TRα1^{L400R} expression in PV neurons. a RNA-seq analysis of nuclear transcriptome of PV neurons. The heatmap represents the variation in gene expression (blue: downregulation, orange: upregulation) of the 281 genes that are differentially expressed in *Thra$^{AMI/+}$ ROSA-GSL10gfp^{lox} Pvalb-Cre* mice (mut, n = 4) and *Thra$^{+/+}$ ROSA-GSL10gfp^{lox} Pvalb-Cre* control littermates (ctrl, n = 4). Although less visible, hypothyroidism has a similar influence on their expression level (hypoth., n = 4). TH treatment tends to restore the original level of gene expression, although only partially after 24 hours (+TH; n = 4). Blue arrows indicate the 12 genes for which Atac-seq indicates a modification of chromatin accessibility caused by the binding of TH to TRs in a sequence located within 30 kb of the transcription start site (see text). **b** Overlap between the responses to TRα1^{L400R} expression, hypothyroidism and TH treatment of hypothyroid mice, as evidenced by RNA-seq analysis. The numbers represent the genes that are down-regulated by reduced thyroid signaling and/or up-regulated upon TH treatment. Here we applied a threshold of 1.5 for fold-changes (blue: down-regulated, orange: upregulated). Note that 24 hours of TH treatment is not sufficient for a full restoration of gene expression in hypothyroid mice. **c** Same analysis for genes that are up-regulated by reduced thyroid signaling and/or down-regulated upon TH treatment. **d** An example of Atac-seq results next to the *Sema7a* gene. The likely position of TR binding sites in PV neurons are boxed. Note the influence of TH treatment on peak height, which is statistically significant for the two boxed peaks.

Fig. 2 | Parvalbumin and PNN alterations in PV neurons expressing TRα1^{L400R} in the somatosensory cortex. a Immunohistochemistry of parvalbumin and WFA-labeled PNNs in PV neurons of somatosensory cortex. **b** The density of Tomato+ cells in *Thra$^{AMI/+}$ ROSA-tdTomato$^{lox/+}$ Pvalb-Cre* mice (n = 9) did not differ from that in *Thra$^{+/+}$ ROSA-tdTomato$^{lox/+}$ Pvalb-Cre* control littermates (n = 7). **c** The density of parvalbumin+ cells was slightly, but significantly, higher in mutants. **d** The density of PNN+ cells did not differ between the two groups. **e** The proportion of PV neurons surrounded by PNNs was slightly, but significantly lower in mutants. Data are presented as mean ± SEM and analyzed using unpaired two-tailed T-test (*$p < 0.05$, **$p < 0.01$, ***$p < 0.001$).

Fig. 3 | Electrophysiological alterations in PV neurons expressing TRα1^{L400R} in the somatosensory cortex. a Current-clamp recordings of a control (*Thra$^{+/+}$ ROSA-tdTomato$^{lox/+}$ Pvalb-Cre*) PV neuron in response to the current pulses (bottom traces) of -100, -80, -60, -40, -20, +140, and +760 pA. Note the short latency of fast action potentials (APs) induced by a just-above-threshold current pulse (140 pA; middle trace). Strong depolarizing current (760 pA; top trace) evoked a high and saturated firing rate. **b** Current-clamp recordings of a mutant (*Thra$^{AMI/+}$ ROSA-tdTomato$^{lox/+}$ Pvalb-Cre*) PV neuron in

response to the current pulses (bottom traces) of -100, -80, -60, -40, -20, +260, and +880 pA. Note the short latency of fast APs induced by a just-above-threshold current pulse (260 pA; middle trace). Strong depolarizing current (880 pA; top trace) evoked a high and saturated firing rate. **c** Rheobase, the minimal current intensity required for AP firing , is higher in mutant PV neurons (n = 35) than that in the controls (n = 19). **d** The threshold of the first two APs induced by the just-above-threshold current pulse in mutant PV neurons (n = 35), are higher than those in the controls (n = 19). Data are presented as mean ± SEM and analyzed using unpaired two-tailed T-test (*$p < 0.05$, **$p < 0.01$, ***$p < 0.001$). Also see Supplementary Table 2 for related analyses and datasets.

Fig. 4 | Behavioral alterations of mice expressing TRα1^{L400R} in PV neurons. a Total distance traveled (m) in the open-field test was longer in mutant (*Thra*$^{AMI/+}$ *Pvalb-Cre*) mice (n = 12) than that in control (*Thra*$^{+/+}$ *Pvalb-Cre*) littermates (n = 12, unpaired two-tailed T-test). **b** The time spent in open arms in the elevated-plus-maze test did not differ between controls (n = 12) and mutants (n = 12, unpaired two-tailed T-test). **c** Touch-screen test: percentage of correct responses of controls (n = 11) and mutants (n = 11) in a visual discrimination task and in a reversal task (one sample T-test, @ $p < 0.05$ vs chance). **d** Novel object recognition test: Exploration time (s) of the object during the acquisition (Acq-) and retention (Ret-) sessions, and recognition index (%) (controls n = 12, mutants n = 12, unpaired two-tailed T-test and one sample T-test, @ $p < 0.05$ vs chance and @@@@ $p < 0.00001$ vs chance). **e** Marble-burying test: percentage of buried marbles (controls n = 12, mutants n = 12, Mann-Whitney test). **f** Social interaction with a newcomer: Social approach number (unpaired two-tailed T-test), contact mean duration (Mann-Whitney test) and contact total duration (unpaired two-tailed T-test) (controls n = 10, mutants n = 11). **g** Pentylenetetrazole-induced seizure test: percentage of mice showing myoclonic, clonic, tonic seizures and death (controls n = 12, mutants n = 12, Chi-square test). Data are presented as mean ± SEM and analyzed using the indicated tests (*$p < 0.05$, **$p < 0.01$, ***$p < 0.001$). Also see Supplementary Table 2 for related analyses and datasets.

Acknowledgements:

We thank Hugues Jacobs, Olivia Wendling, Emel Laghouati, Tania Sorg-Guss and Yann Hérault for the behavioral tests performed at Mouse Clinical Institute (Strasbourg, France). We acknowledge the contributions of the CELPHEDIA Infrastructure (http://www.celphedia.eu/), especially the center AniRA in Lyon. We acknowledge the contribution of SFR Biosciences (Université Claude Bernard Lyon 1, CNRS UAR3444, Inserm US8, ENS de Lyon): Nadine Aguilera and the Plateau de Biologie Expérimentale de la Souris (ANIRA-PBES) for mouse breeding ; ANIRA-CYTOMETRIE and particularly Sébastien Dussurgey for nuclei sorting ; ANIRA-AGC for mouse genotyping. We acknowledge Benjamin Gillet and Sandrine Hughes of the deep sequencing facility (PSI IGFL, Lyon). We also thank Isabelle Dusart (Institut de Biologie Paris Seine, France) for helpful discussions. We acknowledge China Scholarship Council for a scholarship to Juan REN to do her PhD project in ENS de Lyon. Research fundings were from European Union's Horizon 2020 research and innovation program, under grant agreement No. 825753 (ERGO), Agence Nationale de la Recherche (Thyromut2 program; ANR-15-CE14-0011-01) and the PHENOMIN program.

Authors contribution

Conceptualization: S.R., F.F., B.C., F.R. Investigation : J.R., R.G., D.A., R.G., S.M., D.L. Writing- Original Draft : J.R., F.F. Writing – Review & Editing: All authors. Funding Acquisition: F.F., J.W. Supervision: S.R., F.F., D.L., B.C.

Declaration of interest

No conflict of interest

References

Anders, S., Pyl, P.T., and Huber, W. (2015). HTSeq--a Python framework to work with high-throughput sequencing data. Bioinformatics *31*, 166-169.

Ascoli, G.A., Alonso-Nanclares, L., Anderson, S.A., Barrionuevo, G., Benavides-Piccione, R., Burkhalter, A., Buzsaki, G., Cauli, B., Defelipe, J., Fairen, A.*, et al.* (2008). Petilla terminology: nomenclature of features of GABAergic interneurons of the cerebral cortex. Nat Rev Neurosci *9*, 557-568.

Berbel, P., Marco, P., Cerezo, J.R., and DeFelipe, J. (1996). Distribution of parvalbumin immunoreactivity in the neocortex of hypothyroid adult rats. Neurosci Lett *204*, 65-68.

Bode, H., Ivens, B., Bschor, T., Schwarzer, G., Henssler, J., and Baethge, C. (2021). Association of Hypothyroidism and Clinical Depression A Systematic Review and Meta-analysis. Jama Psychiat *78*, 1375-1383.

Burckstummer, T., Bennett, K.L., Preradovic, A., Schutze, G., Hantschel, O., Superti-Furga, G., and Bauch, A. (2006). An efficient tandem affinity purification procedure for interaction proteomics in mammalian cells. Nat Methods *3*, 1013-1019.

Chatonnet, F., Picou, F., Fauquier, T., and Flamant, F. (2011). Thyroid hormone action in cerebellum and cerebral cortex development. Journal of thyroid research *2011*, 145762.

Cho, Y.W., Fu, Y., Huang, C.J., Wu, X., Ng, L., Kelley, K.A., Vella, K.R., Berg, A.H., Hollenberg, A.N., Liu, H.*, et al.* (2023). Thyroid hormone-regulated chromatin landscape and transcriptional sensitivity of the pituitary gland. Commun Biol *6*, 1253.

de Chaumont, F., Ey, E., Torquet, N., Lagache, T., Dallongeville, S., Imbert, A., Legou, T., Le Sourd, A.M., Faure, P., Bourgeron, T.*, et al.* (2019). Real-time analysis of the behaviour of groups of mice via a depth-sensing camera and machine learning. Nat Biomed Eng *3*, 930-942.

de Lecea, L., del Rio, J.A., and Soriano, E. (1995). Developmental expression of parvalbumin mRNA in the cerebral cortex and hippocampus of the rat. Brain Res Mol Brain Res *32*, 1-13.

Deacon, R.M. (2006). Digging and marble burying in mice: simple methods for in vivo identification of biological impacts. Nature protocols *1*, 122-124.

del Rio, J.A., de Lecea, L., Ferrer, I., and Soriano, E. (1994). The development of parvalbumin-immunoreactivity in the neocortex of the mouse. Brain Res Dev Brain Res *81*, 247-259.

Ettleson, M.D., Raine, A., Batistuzzo, A., Batista, S.P., McAninch, E., Teixeira, M.C.T.V., Jonklaas, J., Laiteerapong, N., Ribeiro, M.O., and Bianco, A.C. (2022). Brain Fog in Hypothyroidism: Understanding the Patient's Perspective. Endocrine Practice *28*, 257-264.

Fehling, H.J., Lacaud, G., Kubo, A., Kennedy, M., Robertson, S., Keller, G., and Kouskoff, V. (2003). Tracking mesoderm induction and its specification to the hemangioblast during embryonic stem cell differentiation. Development *130*, 4217-4227.

Hadjab-Lallemend, S., Wallis, K., van Hogerlinden, M., Dudazy, S., Nordstrom, K., Vennstrom, B., and Fisahn, A. A mutant thyroid hormone receptor alpha1 alters hippocampal circuitry and reduces seizure susceptibility in mice. Neuropharmacology *58*, 1130-1139.

Heiman, M., Schaefer, A., Gong, S., Peterson, J.D., Day, M., Ramsey, K.E., Suarez-Farinas, M., Schwarz, C., Stephan, D.A., Surmeier, D.J.*, et al.* (2008). A translational profiling approach for the molecular characterization of CNS cell types. Cell *135*, 738-748.

Hippenmeyer, S., Vrieseling, E., Sigrist, M., Portmann, T., Laengle, C., Ladle, D.R., and Arber, S. (2005). A developmental switch in the response of DRG neurons to ETS transcription factor signaling. PLoS Biol *3*, e159.

Hochbaum, D.R., Dubinsky, A.C., Farnsworth, H.C., Hulshof, L., Kleinberg, G., Urke, A., Wang, W., Hakim, R., Robertson, K., Park, C.*, et al.* (2023). Thyroid hormone rewires cortical circuits to coordinate body-wide metabolism and exploratory drive. bioRxiv.

Hu, H., Gan, J., and Jonas, P. (2014). Interneurons. Fast-spiking, parvalbumin(+) GABAergic interneurons: from cellular design to microcircuit function. Science *345*, 1255263.

Karagiannis, A., Gallopin, T., David, C., Battaglia, D., Geoffroy, H., Rossier, J., Hillman, E.M., Staiger, J.F., and Cauli, B. (2009). Classification of NPY-expressing neocortical interneurons. J Neurosci *29*, 3642-3659.

Langmead, B., Trapnell, C., Pop, M., and Salzberg, S.L. (2009). Ultrafast and memory-efficient alignment of short DNA sequences to the human genome. Genome Biol *10*, R25.

Love, M.I., Huber, W., and Anders, S. (2014). Moderated estimation of fold change and dispersion for RNA-seq data with DESeq2. Genome Biol *15*, 550.

Madisen, L., Zwingman, T.A., Sunkin, S.M., Oh, S.W., Zariwala, H.A., Gu, H., Ng, L.L., Palmiter, R.D., Hawrylycz, M.J., Jones, A.R.*, et al.* (2010). A robust and high-throughput Cre reporting and characterization system for the whole mouse brain. Nat Neurosci *13*, 133-140.

Metsalu, T., and Vilo, J. (2015). ClustVis: a web tool for visualizing clustering of multivariate data using Principal Component Analysis and heatmap. Nucleic Acids Res *43*, W566-570.

Ng, L., Liu, H., Liu, Y., and Forrest, D. (2023). Biphasic expression of thyroid hormone receptor TRbeta1 in mammalian retina and anterior ocular tissues. Frontiers in endocrinology *14*, 1174600.

Picou, F., Fauquier, T., Chatonnet, F., Richard, S., and Flamant, F. (2014). Deciphering direct and indirect influence of thyroid hormone with mouse genetics. Mol Endocrinol *28*, 429-441.

Quignodon, L., Vincent, S., Winter, H., Samarut, J., and Flamant, F. (2007). A point mutation in the activation function 2 domain of thyroid hormone receptor alpha1 expressed after CRE-mediated recombination partially recapitulates hypothyroidism. Mol Endocrinol *21*, 2350-2360.

Richard, S., Guyot, R., Rey-Millet, M., Prieux, M., Markossian, S., Aubert, D., and Flamant, F. (2020). A Pivotal Genetic Program Controlled by Thyroid Hormone during the Maturation of GABAergic Neurons. iScience *23*, 100899.

Rubenstein, J.L., and Merzenich, M.M. (2003). Model of autism: increased ratio of excitation/inhibition in key neural systems. Genes Brain Behav *2*, 255-267.

Rudy, B., Fishell, G., Lee, S., and Hjerling-Leffler, J. (2011). Three groups of interneurons account for nearly 100% of neocortical GABAergic neurons. Dev Neurobiol *71*, 45-61.

Sohal, V.S., and Rubenstein, J.L.R. (2019). Excitation-inhibition balance as a framework for investigating mechanisms in neuropsychiatric disorders. Mol Psychiatry *24*, 1248-1257.

Sorg, B.A., Berretta, S., Blacktop, J.M., Fawcett, J.W., Kitagawa, H., Kwok, J.C., and Miquel, M. (2016). Casting a Wide Net: Role of Perineuronal Nets in Neural Plasticity. J Neurosci *36*, 11459-11468.

Venero, C., Guadano-Ferraz, A., Herrero, A.I., Nordstrom, K., Manzano, J., de Escobar, G.M., Bernal, J., and Vennstrom, B. (2005). Anxiety, memory impairment, and locomotor dysfunction caused by a mutant thyroid hormone receptor {alpha}1 can be ameliorated by T3 treatment. Genes Dev *19*, 2152-2163.

Wallis, K., Dudazy, S., van Hogerlinden, M., Nordstrom, K., Mittag, J., and Vennstrom, B. (2010). The thyroid hormone receptor alpha1 protein is expressed in embryonic postmitotic neurons and persists in most adult neurons. Mol Endocrinol *24*, 1904-1916.

Wallis, K., Sjogren, M., van Hogerlinden, M., Silberberg, G., Fisahn, A., Nordstrom, K., Larsson, L., Westerblad, H., Morreale de Escobar, G., Shupliakov, O*., et al.* (2008). Locomotor deficiencies and aberrant development of subtype-specific GABAergic interneurons caused by an unliganded thyroid hormone receptor alpha1. J Neurosci *28*, 1904-1915.

Zekri, Y., Guyot, R., and Flamant, F. (2022). An Atlas of Thyroid Hormone Receptors' Target Genes in Mouse Tissues. International journal of molecular sciences *23*.

Zhang, W.J., Shi, H.Z., Guo, M.N., Xu, L.F., Zhai, H.R., Liu, Z.Z., Zhu, Y.Q., Zhang, W.N., and Wang, J. (2023). PGC-1alpha regulates critical period onset/closure, mediating cortical plasticity. Front Mol Neurosci *16*, 1149906.

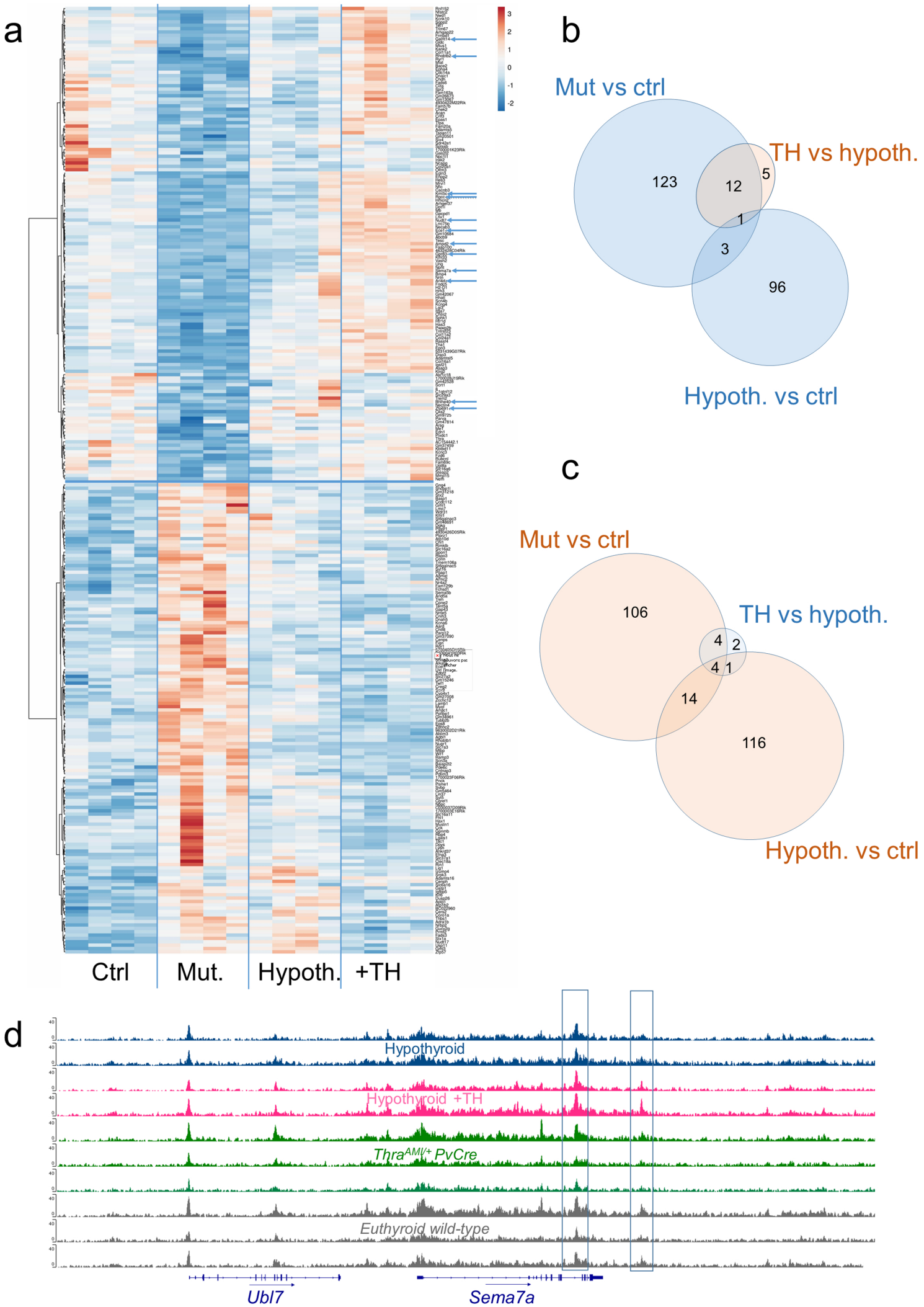
a
Ctrl
Mut.
Hypoth.
+TH
b
Mut vs ctrl
TH vs hypoth.
Hypoth. vs ctrl
123
12
5
1
3
96
c
Mut vs ctrl
TH vs hypoth.
Hypoth. vs ctrl
106
4
2
4
1
14
116
d
Hypothyroid
Hypothyroid +TH
Thra^AM/+ PvCre
Euthyroid wild-type
Ubl7
Sema7a

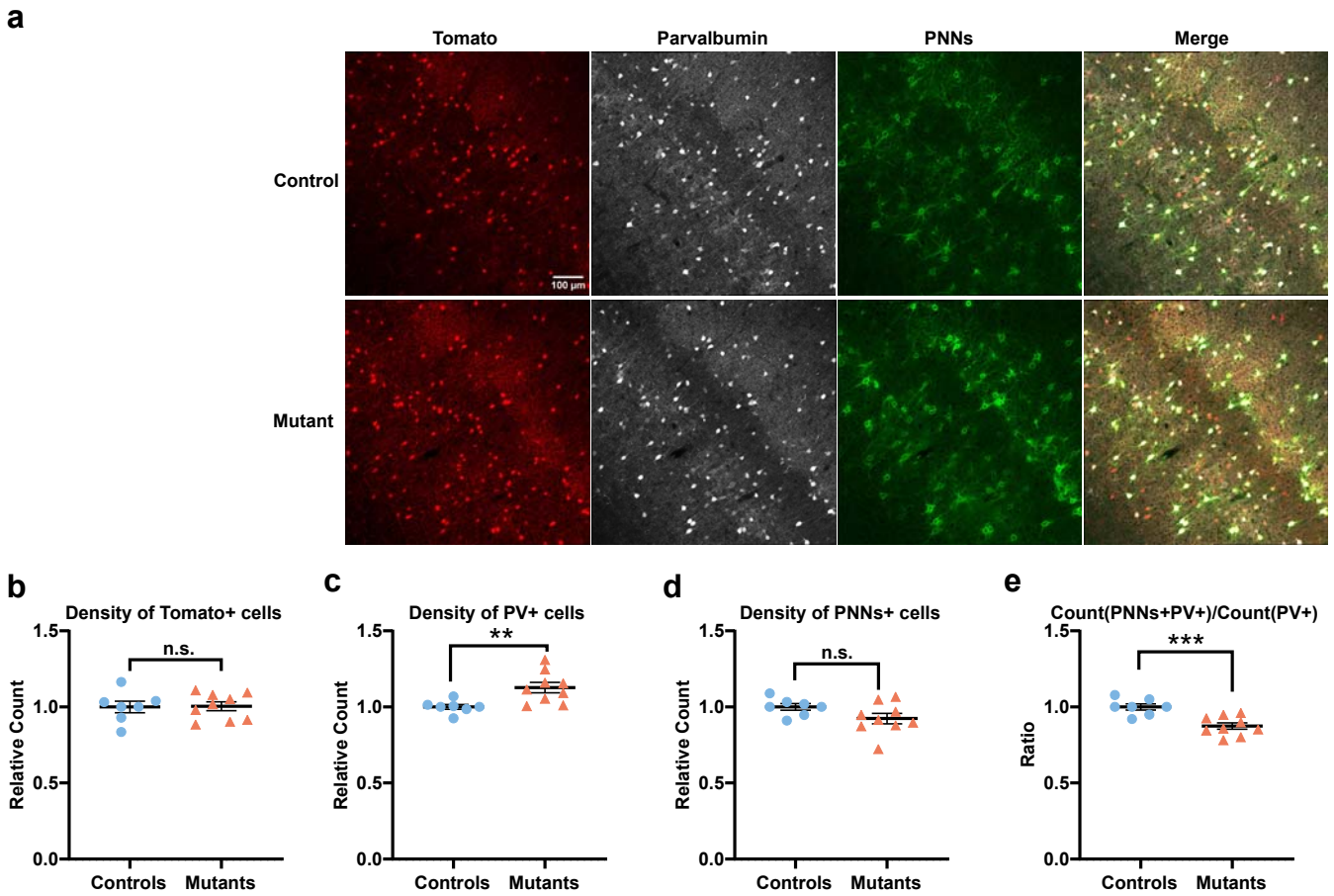
a
Tomato
Parvalbumin
PNNs
Merge
Control
Mutant
100 µm
b
Density of Tomato+ cells
n.s.
Relative Count
1.5
1.0
0.5
0.0
Controls
Mutants
c
Density of PV+ cells
**
Relative Count
Controls
Mutants
d
Density of PNNs+ cells
n.s.
Relative Count
Controls
Mutants
e
Count(PNNs+PV+)/Count(PV+)
***
Ratio
Controls
Mutants

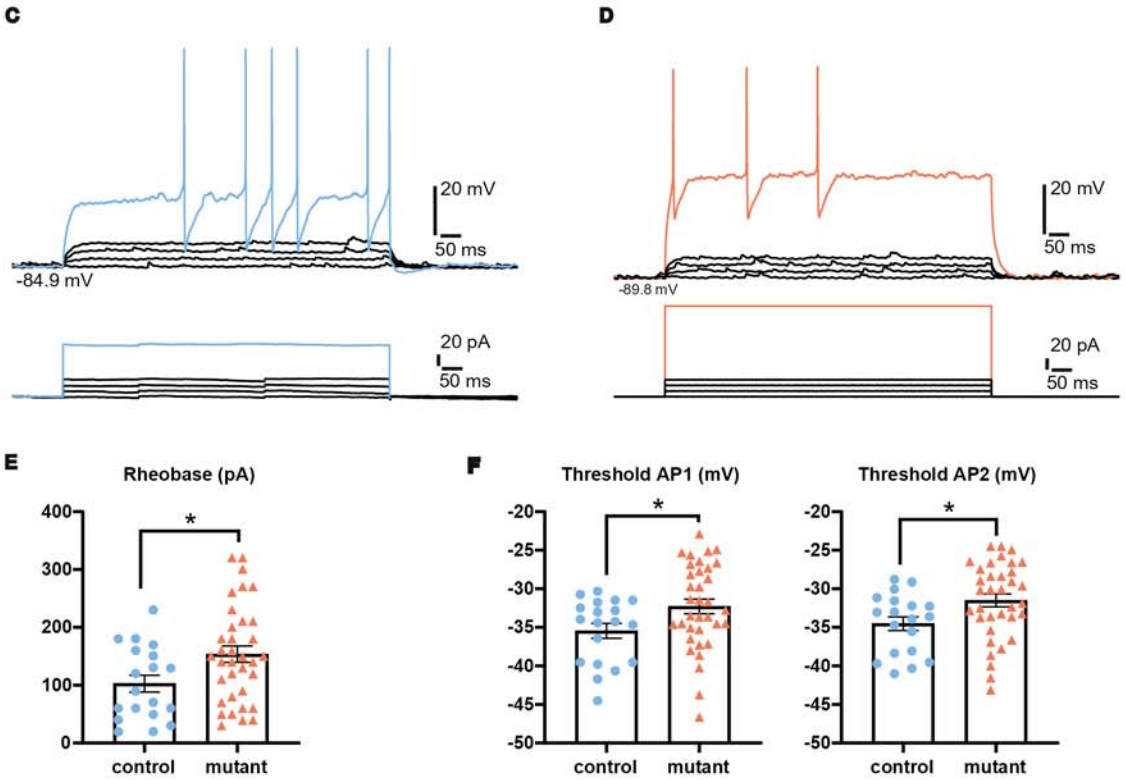
C
20 mV
50 ms
-84.9 mV
20 pA
50 ms
D
20 mV
50 ms
-89.8 mV
20 pA
50 ms
E
Rheobase (pA)
400
300
200
100
0
*
control
mutant
F
Threshold AP1 (mV)
-20
-25
-30
-35
-40
-45
-50
*
control
mutant
Threshold AP2 (mV)
-20
-25
-30
-35
-40
-45
-50
*
control
mutant

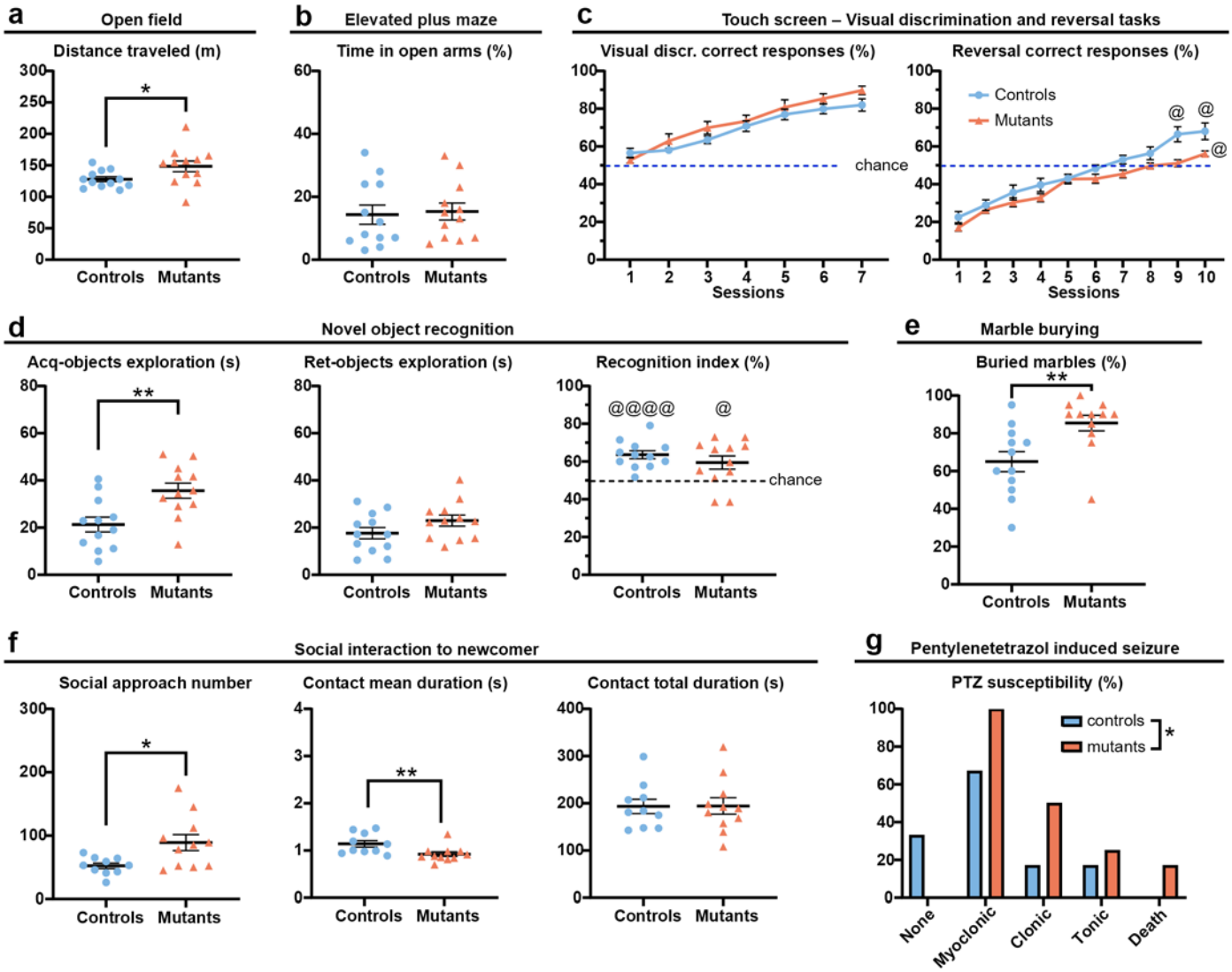
a
Open field
Distance traveled (m)
Controls
Mutants
b
Elevated plus maze
Time in open arms (%)
Controls
Mutants
c
Touch screen – Visual discrimination and reversal tasks
Visual discr. correct responses (%)
chance
Sessions
Reversal correct responses (%)
Controls
Mutants
Sessions
d
Novel object recognition
Acq-objects exploration (s)
Ret-objects exploration (s)
Recognition index (%)
chance
Controls
Mutants
e
Marble burying
Buried marbles (%)
Controls
Mutants
f
Social interaction to newcomer
Social approach number
Contact mean duration (s)
Contact total duration (s)
Controls
Mutants
g
Pentylenetetrazol induced seizure
PTZ susceptibility (%)
controls
mutants
None
Myoclonic
Clonic
Tonic
Death

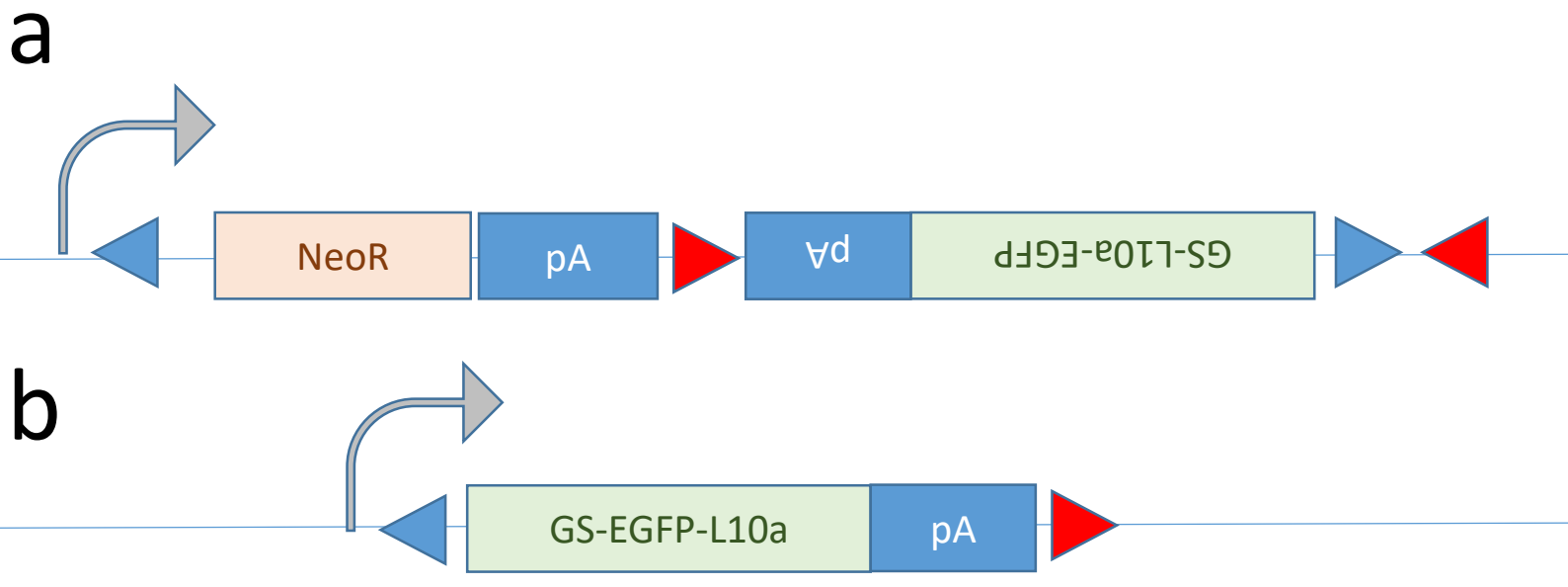

Suppl. Fig1: map of the *ROSA-GSL10gfp*^{lox}

a. Before Cre/loxP recombination the ROSA promoter drive the expression of the NeoR drug resistance gene.

b. After a two step recombination mediated by the Cre recombinase between LoxP (blue) and loxP2272 (red) sequences, the fragment encoding NeoR is deleted and the fragment encoding the GS-EGFP-L10a fusuion protein is inverted. This result is the expression of a fluorescent protein which is predominantly nuclear.

Supplementary Table 1. Statistical result for 26 essential electrophysiological parameters. Control n = 19, Mutant n = 35.

Phase	Parameters	mean ± SEM		P value	
		Control	Mutant	T-test	Mann-Whitney
Subthreshold properties	RMP (mV)	-78.68 ± 1.83	-80.70 ± 0.94		0.72
	R_m (MΩ)	269.20 ± 33.08	202.69 ± 16.18		0.12
	t_{IC} (ms)	15.32 ± 2.40	12.61 ± 0.84		0.29
	C_m (pF)	63.47 ± 7.45	68.06 ± 3.94		0.20
	Δ G_{sag} (%)	0.08 ± 0.02	0.09 ± 0.01		0.51
Near threshold properties	**Rheobase (pA)**	**102.71 ± 14.57**	**153.66 ± 14.05**	**0.02 ***	
	1st spike delay (ms)	277.42 ± 58.54	183.11 ± 35.87		0.20
	$m_{threshold}$ (Hz/s)	-18.97 ± 12.52	-26.89 ± 10.70		0.83
	$C_{threshold}$ (Hz)	23.21 ± 3.80	29.44 ± 3.91		0.38
	Hump (mV)	0.86 ± 0.15	0.63 ± 0.06		0.30
Saturating properties	A_{sat} (Hz)	34.10 ± 2.15	28.16 ± 3.23	0.21	
	t_{sat} (ms)	26.84 ± 7.37	59.38 ± 21.26		0.92
	C_{sat} (Hz)	170.02 ± 10.60	165.80 ± 9.17	0.78	
	m_{sat} (Hz/s)	-28.81 ± 3.45	-32.63 ± 4.16		0.98
Action Potential Waveform	A1 (mV)	54.83 ± 1.49	51.72 ± 1.65	0.22	
	AHP1f (mV)	-26.01 ± 0.68	-26.48 ± 0.64	0.64	
	T_{AHP1f} (ms)	2.63 ± 0.19	2.38 ± 0.14	0.27	
	D1 (ms)	0.61 ± 0.03	0.57 ± 0.03		0.14
	Threshold AP1 (mV)	**-35.45 ± 0.97**	**-32.28 ± 0.94**	**0.04 ***	
	A2 (mV)	53.23 ± 1.28	50.58 ± 1.44	0.23	
	AHP2f (mV)	-26.48 ± 0.65	-27.23 ± 0.56	0.41	
	T_{AHP2f} (ms)	2.62 ± 0.16	2.45 ± 0.15		0.30
	D2 (ms)	0.62 ± 0.03	0.57 ± 0.03		0.13
	Threshold AP2 (mV)	**-34.52 ± 0.90**	**-31.51 ± 0.84**	**0.03 ***	
	Amp, Red,	0.03 ± 0.01	0.02 ± 0.01	0.58	
	Dur, Inc,	0.02 ± 0.01	0.01 ± 0.00		0.46

Supplementary Table 2. Statistical result for the key parameters in each behavioral test.
Note: 2 groups of mice underwent different tests sequentially.

Age (week)	Test	Parameters	Control		Mutant		P value	
			N	Mean ± SEM	N	Mean ± SEM	T-test	Mann-Whitney
17	Open Field	Distance traveled (m)	12	127.95 ± 10.49	12	148.40 ± 8.54	**0.04** *	
		Number of rearings	12	219.25 ± 15.71	12	270.33 ± 21.64	0.07	
		% Time in center	12	21.46 ± 1.30	12	24.95 ± 2.02		0.36
		Entries in center	12	198.08 ± 7.03	12	241.42 ± 12.55	**0.006** **	
		Distance in center (m)	12	43.88 ± 3.80	12	54.75 ± 3.88	**0.02** *	
		Distance in periphery (m)	12	84.07 ± 7.23	12	93.65 ± 6.87	0.23	
17	Elevated Plus Maze	Open Arm Entries	12	4.67 ± 0.63	12	5.08 ± 0.65	0.65	
		Closed Arm Entries	12	11.92 ± 0.84	12	12.92 ± 0.87	0.42	
		Total Arm Entries	12	16.58 ± 1.12	12	18.00 ± 1.27	0.41	
		% Open Entries	12	27.42 ± 2.84	12	27.67 ± 2.49	0.95	
		Attempts	12	20.75 ± 2.12	12	25.67 ± 1.44	0.07	
		Head-Dips	12	6.92 ± 1.12	12	5.00 ± 0.99	0.21	
		Stretched-Attend Posture	12	6.08 ± 0.72	12	6.33 ± 0.72	0.81	
		Open Arm Entry Latency (s)	12	25.78 ± 9.29	12	40.05 ± 20.43		0.88
		Open Time (s)	12	43.08 ± 9.19	12	46.17 ± 8.01	0.80	
		Closed Time (s)	12	154.83 ± 5.66	12	147.75 ± 9.91	0.54	
		Center Time (s)	12	102.50 ± 8.87	12	106.75 ± 7.92	0.72	
		% Time in Open Arms	12	14.33 ± 3.04	12	15.33 ± 2.68	0.81	
		% Open Entries / (Open + Closed)	12	20.42 ± 3.83	12	23.67 ± 3.86	0.56	
		Open Arm Time (proximal)	12	19.50 ± 2.93	12	21.08 ± 2.27		0.60
		Open Arm Time (distal)	12	23.42 ± 7.25	12	24.92 ± 7.33		> 0.99
18-22	Touch Screen	Nb of trials before criterion for Visual Discrimination	10	162 ± 15.62	12	130 ± 19.31		0.19
		Nb of trials before criterion for Reversal Task	11	517.36 ± 24.10	11	583.73 ± 8.16		**0.03** *
23	Novel Object Recognition	Habituation Distance Traveled (m)	12	35.70 ± 1.32	12	45.35 ± 3.93	**0.03** *	
		Acquisition Distance Traveled (m)	12	23.72 ± 1.28	12	29.76 ± 2.45		**0.04** *
		Retention Distance Traveled (m)	12	18.67 ± 0.99	12	23.33 ± 2.53		**0.03** *

24	Marble Burying	% Buried marbles (15 min)	12	65.00 ± 5.33	12	85.42 ± 4.15		**0.005 ****
25	Social Interaction	Habituation Total Distance (m)	10	77.60 ± 2.76	11	95.33 ± 8.24		**0.04 ***
		Habituation Center Distance (m)	10	13.16 ± 0.96	11	19.14 ± 3.17		0.0845
		Habituation % Distance in Center	10	16.78 ± 0.79	11	19.25 ± 1.59	0.1946	
		Habituation Center Time (s)	10	97.36 ± 5.92	11	122.25 ± 13.74	0.1251	
		Habituation % Time in Center	10	8.11 ± 0.49	11	10.19 ± 1.15	0.1251	
		Distance traveled (m)	10	99.24 ± 4.13	10	133.30 ± 13.53	**0.003 ****	
		Social Approach Nb	10	52.30 ± 4.37	11	89.00 ± 12.59	**0.02 ***	
		Social Approach Mean Duration (s)	10	0.70 ± 0.03	11	0.73 ± 0.04	0.55	
		Social Approach Total Duration (s)	10	36.72 ± 3.51	11	66.84 ± 11.90		0.05
		Contact Nb	10	170.20 ± 9.66	11	210.55 ± 15.46	**0.04 ***	
		Contact Mean Duration (s)	10	1.14 ± 0.07	11	0.92 ± 0.05		**0.006 ****
		Contact Total Duration (s)	10	193.35 ± 15.29	11	194.32 ± 17.60	0.97	
		Oral-Genital Nb	10	78.10 ± 7.61	11	97.91 ± 8.83	0.11	
		Oral-Genital Mean Duration (s)	10	0.39 ± 0.01	11	0.37 ± 0.02	0.39	
		Oral-Genital Total Duration (s)	10	30.01 ± 2.70	11	35.72 ± 3.43	0.21	
		Oral-Oral Nb	10	83.60 ± 7.58	11	86.09 ± 7.50	0.82	
		Oral-Oral Mean Duration (s)	10	0.45 ± 0.02	11	0.43 ± 0.02	0.27	
		Oral-Oral Total Duration (s)	10	37.45 ± 2.96	11	35.97 ± 2.50	0.71	
		Side by Side Nb	10	44.60 ± 6.37	11	51.00 ± 9.89		0.80
		Side by Side Mean Duration (s)	10	0.42 ± 0.02	11	0.38 ± 0.01	0.06	
		Side by Side Total Duration (s)	10	18.77 ± 2.75	11	19.13 ± 3.53	0.94	
		Follow Nb	10	2.80 ± 0.85	11	5.18 ± 1.27	0.14	
		Follow Mean Duration (s)	10	0.40 ± 0.07	11	0.41 ± 0.05	0.95	
		Follow Total Duration (s)	10	1.34 ± 0.37	11	2.45 ± 0.68	0.18	
33	Pentylenetetrazol induced Seizure	PTZ susceptibility	12		12		**0.05 ***	Chi-square